SHARP Edges: Recovering Cortical Phase Contrast Through Harmonic Extension

Ryan Topfer[1,2], Ferdinand Schweser[3], Andreas Deistung[3], Alan H Wilman[1,2], and Jürgen R Reichenbach[3]

[1]*Department of Physics, University of Alberta, Edmonton, AB, Canada,* [2]*Department of Biomedical Engineering, University of Alberta, Edmonton, AB, Canada,*
[3]*Medical Physics Group, Institute of Diagnostic and Interventional Radiology I, Jena University Hospital - Friedrich Schiller University, Jena, Thuringia, Germany*

Target Audience: Researchers interested in phase imaging and quantitative susceptibility mapping (QSM).

Purpose: Gradient echo (GRE) phase is increasingly being studied given its sensitivity to the magnetic properties of tissue. However, in its unprocessed form, the measured phase is overwhelmed by contributions from susceptibility sources external to tissue. Two novel approaches to the issue of background phase removal have recently been published: Sophisticated Harmonic Artifact Reduction for Phase Data (SHARP)[1] and Projection Onto Dipole Fields (PDF)[2]. Unlike traditional high-pass filtering, these methods take advantage of fundamental physical properties of the background phase in order to isolate it and subtract it from measurement. However, a common pitfall to the two techniques is their failure to accurately map local phase near the edges of the brain (e.g. cortex). This is a considerable obstacle in many imaging applications as it precludes analysis of clinically important regions including pial vessels, subdural hematoma, and cortical lesions in pathologies such as multiple sclerosis. To recover this local phase throughout the region of interest, this study presents an extension to conventional SHARP whereby another fundamental property of the background field is used, namely, its analyticity. The proposed method was quantitatively assessed and qualitatively demonstrated using a numerical "field-forward" experiment and *in vivo* data, respectively.

Theory: SHARP takes advantage of the background field being harmonic within the ROI (i.e. brain) by means of the spherical mean value (SMV) property: The average of a harmonic function over the surface of a sphere is equal to the value of the function at the sphere's center. However, a problem occurs wherever the sphere overlaps the ROI boundary (where the background field ceases to be harmonic). Previously, these problematic voxels were simply discarded outright, leaving reliable field information strictly within a *reduced ROI*, and resulting in the loss of field information in the edge regions. Fortunately, since the background field is harmonic, it is *ipso facto* analytic[3], meaning that, within a neighbourhood around a point belonging to the reduced ROI (*internal point*; IP), the background field is equal to its Taylor series representation (Equation 1). Hence, using SHARP to arrive at an initial estimate of the background field, one can then perform a Taylor expansion to extend the field coverage to the hitherto lost voxels at the edges (*edge points*; EP).

Methods: Data acquisition and pre-processing: Whole-head 3D GRE data were acquired at 4.7T (Varian, Palo Alto, CA). Acquisition parameters: FOV = 256x160x160 mm, spatial resolution = 1.0x1.0x2.0 mm; bandwidth = 90.1 kHz; TR = 40ms; TE = 3/7/11/15/19 ms; flip angle = 10°. Images from individual echoes and receiver elements (4-channel array) were combined[4], followed by phase unwrapping using FSL Prelude[5]. Magnitude data were then passed to FSL's brain extraction tool[6].

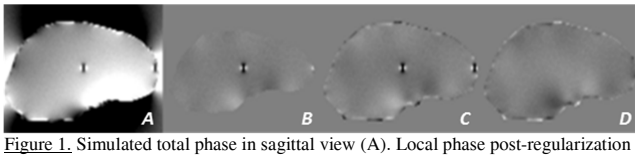

Figure 1. Simulated total phase in sagittal view (A). Local phase post-regularization ($\lambda_{TSVD} = 0.05$): of SHARP (B) and of expansion result (C). Difference image (D) between (C) and local model phase (not shown).

$$[1] \quad \varphi^{EP} = \varphi^{IP} + \begin{bmatrix} \varphi^{IP}{}_x \\ \varphi^{IP}{}_y \\ \varphi^{IP}{}_z \end{bmatrix} [d_x \quad d_y \quad d_z] + \frac{1}{2!} [d_x \quad d_y \quad d_z] \begin{bmatrix} \varphi^{IP}{}_{xx} & \varphi^{IP}{}_{xy} & \varphi^{IP}{}_{xz} \\ \varphi^{IP}{}_{yx} & \varphi^{IP}{}_{yy} & \varphi^{IP}{}_{yz} \\ \varphi^{IP}{}_{zx} & \varphi^{IP}{}_{zy} & \varphi^{IP}{}_{zz} \end{bmatrix} \begin{bmatrix} d_x \\ d_y \\ d_z \end{bmatrix}$$

Equation 1: Taylor expansion of the background phase. φ^{EP} denotes the background phase of an EP voxel; φ_i^{IP} denotes the derivative in direction *i (i=x,y,z)* of the background phase evaluated at an IP voxel and φ_{ii}^{IP} denotes second derivatives accordingly; d_i represents the EP-to-IP distance in the *i* direction.

Numerical simulation: The model was created by assigning the FSL brain mask a water-like susceptibility of -9.4 ppm, while assigning the region external to it an air-like value of 0. This arrangement was to represent the air-tissue interface responsible for the background field. Two *internal* susceptibility inclusions (susceptibility = -9.0 ppm; radii = 2 mm), simulating small spherical hemorrhages, were placed within the brain substrate: one at the center of the brain (IP-region), and one directly at the edge, such that it would be discarded post-SHARP (EP-region). The susceptibility model was convolved with the unit dipole field to simulate the magnetic field, and scaled to phase by multiplicative factor $\gamma B_o TE$ (TE = 19ms), to which zero-mean Gaussian noise was added (standard deviation = π/4 rad, chosen to resemble *in vivo* phase measurement) (Fig. 1, A). In addition, for the purpose of error analysis, the local susceptibility inclusions were used to generate the local model phase on its own, free of noise and background phase.

Data processing: For both *in vivo* and numerical data, phase (masked and unwrapped) was SMV filtered (radius 6 mm), eroded by the radius of the spherical kernel, and finally deconvolved without regularization. These local phase estimates (e.g. Fig 2, A) were subtracted from the unwrapped (total) phase to provide estimates of the background over the reduced brain volume. The hitherto lost EP voxels were paired with their nearest IP neighbours for which 1st and 2nd order spatial derivatives of the phase could be estimated via finite differences. Using these derivatives and the IP-to-EP distances, the background phase estimate was extended via a 2nd order 3-dimensional Taylor expansion (Equation 1). The post-expansion background (e.g. Fig. 2, C) was then subtracted out from the unwrapped phase and the result SHARP-regularized ($\lambda_{TSVD} = 0.05$) to yield the local phase over the extended ROI (Fig. 2, B).

Analysis: Accuracy was assessed by looking at the root mean squared-error (RMSE) within the respective ROIs: reduced ROI (IP voxels) for conventional SHARP; and, for the expansion method, the lost EP region – excluding however the single layer of voxels defining the outer edge (overlay in Fig. 2, A) where the background field becomes inharmonic.

Results & Discussion: In the numerical simulation, conventional SHARP had an RMSE over the IP voxels of 2.29 rad, while the noise RMSE over the whole head (IP+EP) was 0.79 rad. The expansion method recovered the edges (21% of the whole ROI) with RMSE = 2.84 rad – albeit greater than that of SHARP, but visual inspection revealed that this was largely due to areas immediately adjacent to the sinuses (not shown) where the crude 2nd order approximation is insufficient. Deviation decreased away from these regions, where it can be seen to produce results almost entirely continuous with those of SHARP (Fig. 2, B).

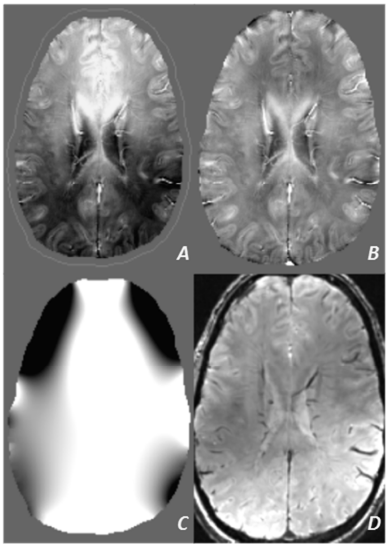

Figure 2. Initial SMV-filtered local phase (A) with overlay of the boundary indicating the EP-region; (C) background field after expansion; (B) local phase after subtracting (C) from the unwrapped phase (not shown) and regularizing ($\lambda_{TSVD} = 0.05$); (D) composite magnitude image.

Conclusion: This study presented an adaptation to the post-processing technique SHARP whereby the analyticity of the background field was used to determine the subset of missing field-map values around the ROI edge. Though the results are with specific reference to SHARP, we surmise the method can be applied equally to PDF.

References: [1] Schweser F, et al. *NeuroImage*. 2011;54(4):2789–807. [2] Liu T, et al. *NMR in biomedicine*. 2011;24(9):1129–36. [3] Richards PI. *Manual of Mathematical Physics*. 1959:316–317. [4] Robinson S, Jovicich J. *Magn Reson Med*. 2011;c:976–988. [5] Jenkinson M. *Magn Reson Med*. 2003;49(1):193–7. [6] Smith SM. *Human brain mapping*. 2002;17(3):143–55.